Probe-corrected near-field measurements on a truncated cylinder[a)]

Thorkild B. Hansen[b)]
Consultant, Air Force Research Laboratory (SNHE), Hanscom AFB, Massachusetts 01731

(Received 3 March 2005; revised 17 November 2005; accepted 18 November 2005)

A probe-corrected theory is presented for computing the acoustic far fields of transducers and scatterers from measurements of near fields on a cylindrical surface. The near-field data is truncated at the top, bottom, and angular edges of the scan cylinder. These truncation edges can cause inaccuracies in the computed far fields. Correction techniques are developed for the top and bottom truncation edges. The cylindrical wave expansions automatically apply an angular taper to the near-field data that reduces the effect of the angular truncation edges. The taper function depends on the probe and the angular sample spacing. The theory is validated through numerical examples involving a point source and a baffled piston transducer probe. © *2006 Acoustical Society of America.* [DOI: 10.1121/1.2151789]

PACS number(s): 43.20.Rz, 43.20.Bi, 43.20.Ye [GCG] Pages: 792–807

I. INTRODUCTION

Probe-corrected near-field techniques have been widely used for the past 40 years to characterize antennas and transducers from measurements on planar,[1–5] cylindrical,[6–10] and spherical[11–20] scanning surfaces. The field of the antenna or transducer is first measured with a known probe on the scanning surface in the near field. Probe-corrected formulas are then applied to the measured near field to get the desired far field of the antenna or transducer. The measurements are typically performed in anechoic chambers. The electromagnetic probe-corrected formulas have been derived and widely implemented for scanning on planar, cylindrical, and spherical surfaces. The corresponding acoustic formulas have only been derived for scanning on planar and spherical surfaces.

The far field of electromagnetic and acoustic scatterers can also be determined from near-field measurements in anechoic chambers.[21–23] A far-field source or a compact-range reflector can provide the plane-wave field required to illuminate or insonify the scatterers. To compute the scattered far field, the incident field and background interactions must be extracted from the measured total field. The simplest method for eliminating these field contributions is standard background subtraction which involves two measurements. The first measurement is carried out with the scatterer present, and the second measurement is carried out with the scatterer removed. The results of the two measurements are then subtracted to get an approximation for the scattered near field, which can be processed with the probe-corrected formulas to get the scattered far field.

It is appropriate to mention the related area of research known as near-field acoustical holography, where near-field measurements are employed to backpropagate the pressure field in space and time toward the source.[24–27] One can achieve super-resolution with near-field holography when part of the evanescent spectrum is captured during the scan. In this paper, however, we are concerned only with computing the field of the source outside the scanning surface and do not attempt to backpropagate the near-field data.

In this paper we derive the probe-corrected formulas for cylindrical near-field scanning that can be used to compute acoustic far fields of transducers and scatterers. We present computation schemes and sampling theorems that allow the far fields to be computed from sampled values of the probe output on the scan cylinder. In practice, the measurements are carried with a mechanical scanner over a truncated scan cylinder that covers only a limited region of the infinite scan cylinder that is used for the derivation. Therefore we carefully examine the probe-corrected formulas to determine how truncation edges may affect the far-field accuracy. We develop edge-correction techniques that reduce the far-field errors caused by truncation and show that an angular taper function is automatically applied to the probe output. The results of the paper are validated through numerical examples involving a point source and a baffled piston transducer probe with a circular cross section.

The paper is organized as follows. In Sec. II we derive the formulas for cylindrical near-field scanning of acoustic fields with an arbitrary known probe. These formulas express the field of the source region in terms of the probe receiving coefficients and the probe output over an infinite scan cylinder. For use in the numerical simulations, we derive exact expressions for the probe output when the probe is a baffled circular receiving piston transducer.

We consider a truncated scan cylinder in Sec. III and develop edge-corrected formulas that compensate for the end-point contributions to the far field from the top and bottom edges. We further study the angular taper function that is inherent in the cylindrical expansions. In Sec. IV the far-field formulas are converted into discrete computation schemes. In Sec. V we consider a point source at the origin to illustrate the implications of truncating the scan cylinder. Section VI presents conclusions.

[a)]Revised version submitted to the Journal of the Acoustical Society of America October 2005. Original manuscript submitted February 2005.
[b)]Electronic mail: Thorkild.Hansen@att.net

 0001-4966/2006/119(2)/792/16/$22.50

REPORT DOCUMENTATION PAGE

Form Approved
OMB No. 0704-0188

PLEASE DO NOT RETURN YOUR FORM TO THE ABOVE ADDRESS.

1. REPORT DATE *(DD-MM-YYYY)*	2. REPORT TYPE	3. DATES COVERED *(From - To)*
01-02-2006	Journal Article	2004

4. TITLE AND SUBTITLE

Probe-corrected near-field measurements on a truncated cylinder

5a. CONTRACT NUMBER

N/A

5b. GRANT NUMBER

N/A

5c. PROGRAM ELEMENT NUMBER

61102F

6. AUTHOR(S)

Thorkild B. Hansen, Consultant
Anteon Corporation
3211 Germantown Rd, Suite 700
Fairfax, VA 22030-2801

5d. PROJECT NUMBER

2304

5e. TASK NUMBER

HE

5f. WORK UNIT NUMBER

2304HE04

7. PERFORMING ORGANIZATION NAME(S) AND ADDRESS(ES)

AFRL/SNHE
80 Scott Drive
Hanscom AFB MA 01731-2909

8. PERFORMING ORGANIZATION REPORT NUMBER

N/A

9. SPONSORING/MONITORING AGENCY NAME(S) AND ADDRESS(ES)

Air Force Research Laboratory
Electromagnetic Scattering Branch
Sensors Directorate
80 Scott Drive,
Hanscom AFB, MA 01731-2909

Source Code: 437890

10. SPONSOR/MONITOR'S ACRONYM(S)

AFRL-SN-HS

11. SPONSOR/MONITOR'S REPORT NUMBER(S)

AFRL-SN-HS-JA-2004-1195

12. DISTRIBUTION/AVAILABILITY STATEMENT

APPROVED FOR PUBLIC RELEASE, DISTRIBUTION UNLIMITED.

13. SUPPLEMENTARY NOTES

ESC Public Affairs Clearance #: 04-1195; Published in Journal Acoustical Society of America, Vol 119 (2), February 2006

14. ABSTRACT

A probe-corrected theory is presented for computing the acoustic far fields of transducers and scatterers from measurements of near fields on a cylindrical surface. The near-field data is truncated at the top, bottom, and angular edges of the scan cylinder. Correction techniques are developed for the top and bottom truncated edges. The cylindrical wave expansions automatically apply an angular taper to the near-field data that reduces the effect of the angular truncation edges. The taper function depends on the probe and angular sample spacing. The theory is validated through numerical examples involving a point source and a baffled piston transducer probe.

15. SUBJECT TERMS

Probe correction, near-field, cylindrical wave expansion

16. SECURITY CLASSIFICATION OF:			17. LIMITATION OF ABSTRACT	18. NUMBER OF PAGES	19a. NAME OF RESPONSIBLE PERSON
a. REPORT	b. ABSTRACT	c. THIS PAGE			RICHARD A. MARR
U	U	U	UU	13	19b. TELEPHONE NUMBER *(Include area code)*

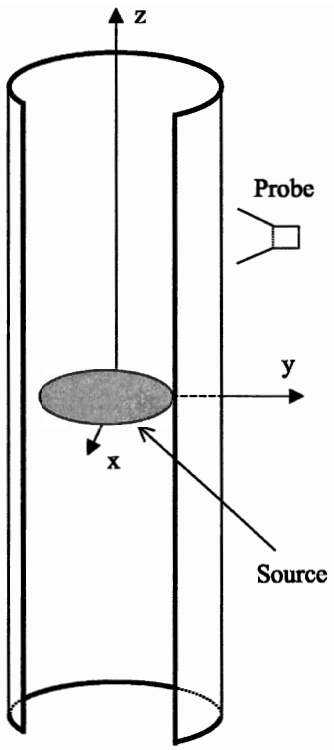

FIG. 1. Probe measures the field of the source on the truncated scan cylinder given by $\rho=a$, $-z_0<z<z_0$, $\phi_0<\phi<2\pi-\phi_0$.

II. THEORY OF CYLINDRICAL NEAR-FIELD SCANNING

We now derive the formulas for computing the acoustic field of a source of finite extent from either the pressure field (Sec. II A) or from the output of a known probe (Sec. II B) on a scan cylinder. The source can either be a transducer or a scatterer. For scatterers we assume that background subtraction has been performed, so that the incident field and background reflections have been removed. The part of space not occupied by the sources is a linear lossless fluid in which the acoustic field can be fully described by its pressure field $p(\mathbf{r})$.

As shown in Fig. 1, the field is measured on the cylinder $\rho=a$, where ρ is the cylindrical coordinate that equals the distance to the z axis. The scan cylinder in Fig. 1 is truncated and covers the region $-z_0\leqslant z\leqslant z_0$, $\phi_0\leqslant\phi\leqslant 2\pi-\phi_0$. For the derivations of this section the scan cylinder is assumed infinite ($z_0=+\infty$ and $\phi_0=0$).

We define the minimum cylinder $\rho=R_{\min}$ such that the maximum (supremum) value of the coordinate ρ for all points on the source equals $R_{\min}$. Note that $R_{\min}$ depends on the size of the source as well as on its location. For example, the value of $R_{\min}$ is equal to $\sqrt{x_1^2+y_1^2}$ for a point source at $(x,y,z)=(x_1,y_1,z_1)$. We assume that the scan cylinder encloses the minimum cylinder.

A. The far field in terms of the field on the scan cylinder

The formulas that express the field from a confined source in terms of the pressure on an enclosing cylinder will be derived in this section from the standard cylindrical wave expansion. With $e^{-i\omega t}$ time dependence suppressed, the basic outgoing solution $p^{(3)}(\mathbf{r})$ to the scalar wave equation

$$(\nabla^2+k^2)p(\mathbf{r})=0 \tag{1}$$

is

$$p^{(3)}(\rho,\phi,z)=H_n^{(1)}(k_\rho\rho)e^{in\phi}e^{ik_z z}, \tag{2}$$

where k is the wave number, k_z is a real parameter, n is an integer, and

$$k_\rho=\sqrt{k^2-k_z^2} \tag{3}$$

is a complex parameter with non-negative real and imaginary parts. Moreover, $H_n^{(1)}(k_\rho\rho)$ is the Hankel function of the first kind and order n, and (ρ,ϕ,z) are the standard cylindrical coordinates given in terms of rectangular coordinates (x,y,z) as

$$x=\rho\cos\phi,\quad y=\rho\sin\phi,\quad z=z. \tag{4}$$

Outside the minimum cylinder of radius $R_{\min}$, the field $p(\mathbf{r})$ of any source of finite extent can be expressed as a superposition of the basis fields in (2) as[28]

$$p(\rho,\phi,z)=\sum_{n=-\infty}^{+\infty}e^{in\phi}\int_{-\infty}^{+\infty}F_n(k_z)H_n^{(1)}(k_\rho\rho)e^{ik_z z}dk_z,$$

$$\rho>R_{\min}, \tag{5}$$

where $F_n(k_z)$ is the spectrum that characterizes the source.

The formula (5) determines the field everywhere outside a cylinder of radius $R_{\min}$ in terms of an integration and a summation involving the spectrum $F_n(k_z)$. By applying the method of stationary phase,[29] one can show that for observation points far form the source the field can be expressed in spherical coordinates as

$$p(r,\theta,\phi)\sim\frac{2e^{ikr}}{r}\sum_{n=-\infty}^{+\infty}F_n(k\cos\theta)e^{in\phi}e^{-i\pi(n+1)/2}, \tag{6}$$

where (r,θ,ϕ) are the standard spherical coordinates related to the rectangular coordinates (x,y,z) through

$$x=r\sin\theta\cos\phi,\quad y=r\sin\theta\sin\phi,\quad z=r\cos\theta. \tag{7}$$

Unlike the general formula (5), the far-field formula (6) does not involve an integration over k_z.

An expression for the spectrum $F_n(k_z)$ in terms of the field $p(a,\phi,z)$ on the scan cylinder is obtained by multiplying Eq. (5) by $e^{-in'\phi}e^{-ik_z' z}$ and integrating over the scan cylinder

$$F_n(k_z)=\frac{1}{4\pi^2H_n^{(1)}(k_\rho a)}\int_{-\infty}^{+\infty}\int_0^{2\pi}p(a,\phi,z)e^{-in\phi}e^{-ik_z z}d\phi dz,$$

$$a>R_{\min}, \tag{8}$$

where we have used the orthogonality relations

$$\int_{-\infty}^{+\infty}e^{i(k_z-k_z')z}dz=2\pi\delta(k_z-k_z') \tag{9}$$

and

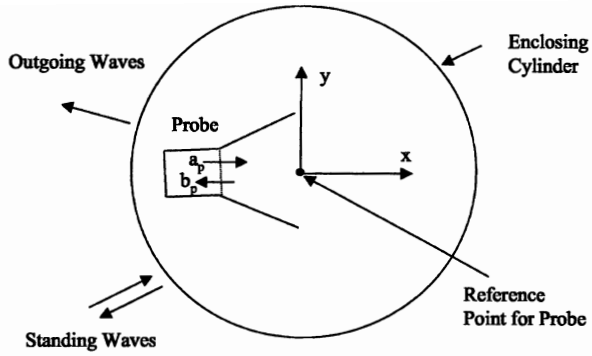

FIG. 2. Probe situated in a probe coordinate system. The input and output of the probe are determined by the mode amplitudes a_p and b_p, respectively. The total field outside the enclosing cylinder for the probe is described in terms of outgoing and standing waves.

$$\int_0^{2\pi} e^{i(n-n')\phi} d\phi = \begin{cases} 2\pi, & n = n' \\ 0, & n \neq n'. \end{cases} \tag{10}$$

Even though the radius a of the scan cylinder appears on the right-hand side of the expression (8) for spectrum, the expression (8) is independent of a. The formulas (5), (6), and (8) express the field everywhere outside a minimum cylinder that encloses the sources in terms of the field on the scan cylinder.

B. Far field in terms of the probe output on the scan cylinder

We shall next present a simple straightforward derivation of the probe-corrected formulas that express the field outside the scan cylinder in terms of the output of a known probe on the scan cylinder. We shall employ the outgoing and standing wave basis functions of the source scattering matrix formulation. The schematic for the cylindrical near-field measurement system is shown in Fig. 1. First we characterize the probe with respect to cylindrical waves.

1. Characterization of the probe

Start by defining a probe coordinate system in which the probe is fixed as shown in Fig. 2. The origin of this coordinate system is the reference point of the probe. The orientation of the probe with respect to a global coordinate system is defined in terms of the orientation of the probe coordinate system with respect to the global coordinate system. For cylindrical scanning we assume that the z axis of the probe coordinate system is parallel to the z axis of the global coordinate system that is used to describe the scanning geometry.

The probe is attached to a waveguide that supports only one propagating mode. The input to the probe is determined by the mode amplitude a_p and the output of the probe is determined by the mode amplitude b_p. We refer to b_p as the probe output and assume that the probe waveguide is perfectly matched ($a_p=0$) when the probe measures the field of the source.

The field outside the cylinder in Fig. 2 that encloses the probe can be described in terms of the outgoing waves

$$p^{(3)}(\rho,\phi,z) = H_n^{(1)}(k_\rho\rho)e^{in\phi}e^{ik_z z} \tag{11}$$

and the standing waves

$$p^{(1)}(\rho,\phi,z) = J_n(k_\rho\rho)e^{in\phi}e^{ik_z z}, \tag{12}$$

where $J_n(k_\rho\rho)$ is the Bessel function of order n. The probe receiving coefficients can now be defined as follows. If the total field outside the enclosing cylinder is the single standing cylindrical wave $J_n(k_\rho\rho)e^{in\phi}e^{ik_z z}$, the probe output is given by $b_p=C_n(kz)$, where $C_n(kz)$ are the probe receiving coefficients.

The probe receiving coefficients will now be expressed in terms of the probe's plane-wave receiving characteristic $R_p(k_x,k_y)$, defined to be the probe output when the incident field is the plane-wave $e^{i(k_x x+k_y y+k_z z)}$, with $k_x^2+k_y^2+k_z^2=k^2$. The plane-wave receiving characteristic, which is also defined with the probe located in the probe coordinate system, can be expressed both in terms of the plane-wave transmitting spectrum and the far-field pattern of the probe when the probe is a reciprocal electroacoustic transducer.[30,5] For example, if the probe is reciprocal and its far field is expressed in terms of a far-field pattern $\mathcal{F}_p(\theta,\phi)$ as $p(\mathbf{r})\sim\mathcal{F}_p(\theta,\phi)e^{ikr}/r$, the receiving characteristic is

$$R_p(k\cos\phi\sin\theta, k\sin\phi\sin\theta) = -\frac{\mathcal{F}_p(\pi-\theta,\pi+\phi)}{i\omega Y_p \rho_{m0}}, \tag{13}$$

where Y_p is the characteristic admittance for the propagating mode of the probe waveguide feed and p_{m0} is the mass density of the undisturbed fluid.

With the angles ϕ_k and θ_k defined such that $k_x=k_\rho\cos\phi_k$, $k_y=k_\rho\sin\phi_k$, and $k_z=k\cos\theta_k$, the cylindrical expansion of the incident plane-wave $e^{i(k_x x+k_y y+k_z z)}$ is

$$e^{i(k_x x+k_y y+k_z z)} = \sum_{n=-\infty}^{+\infty} i^n J_n(k_\rho\rho)e^{in(\phi-\phi_k)}e^{ik_z z}. \tag{14}$$

Note that $k_x<0$ and $\pi/2<\phi_k<3\pi/2$ for plane-wave components generated by sources that are located in the half space $x>0$. By inspection, the plane-wave receiving characteristic is found to be

$$R_p(k_x,k_y) = \sum_{n=-\infty}^{+\infty} i^n C_n(k_z)e^{-in\phi_k}, \tag{15}$$

which in turn yields the desired expression for the receiving coefficients

$$C_n(k_z) = \frac{i^{-n}}{2\pi}\int_0^{2\pi} R_p(k_\rho\cos\phi_k, k_\rho\sin\phi_k)e^{in\phi_k}d\phi_k. \tag{16}$$

As will be demonstrated below, the far field of the source can be determined from the plane-wave receiving characteristic in the region of propagating waves where k_x, k_y, and k_z are real.

2. Piston probe

We consider now a baffled circular receiving piston transducer whose piston resides in the y-z plane of the probe coordinate system. For brevity we shall refer to this receiv-

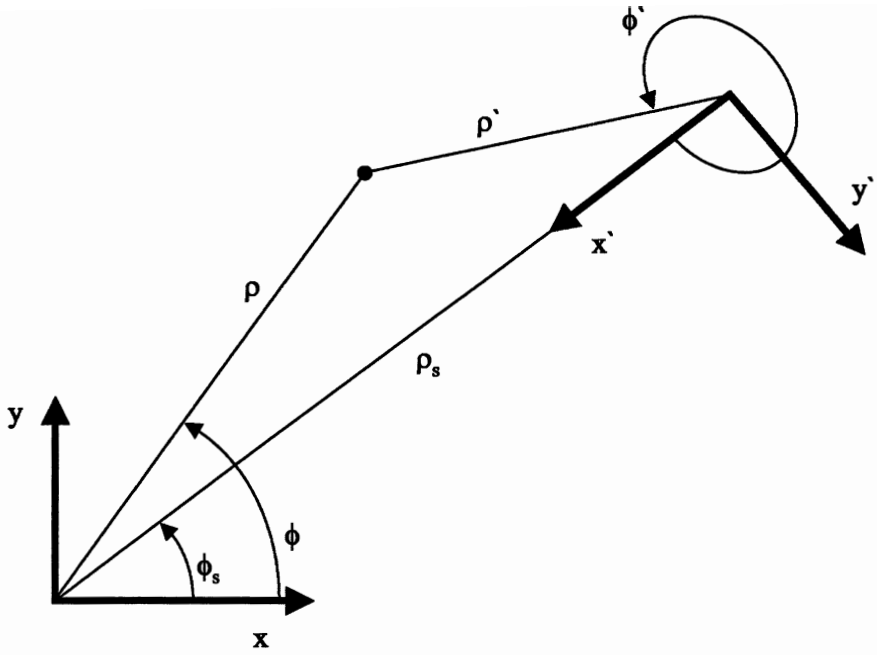

FIG. 5. Geometry for translation and rotation of cylindrical wave functions.

3. Probe-corrected formulas

The probe-corrected formulas for the field of the source will be derived in this section using a straightforward approach that involves two steps. First, an expression is derived for the probe output $b_p(a,\phi,z)$ in terms of the unknown expansion coefficients $F_m(k_z)$ for the source and the known probe receiving coefficients $C_n(k_z)$. Second, this expression for the probe output is inverted to get the expansion coefficients of the source in terms of the probe receiving coefficients and the probe output.

Multiple interactions between the source and the probe will be neglected. That is, the field scattered by the probe, rescattered by the source, and returned to the probe, does not change the output of the probe. The effect of multiple interactions can be taken into account formally by the source scattering matrix formulation.[8] However, this formulation does not provide quantitative information about these multiple interactions, and to obtain useful probe-corrected formulas they have to be neglected.

To derive an expression for the probe output when the probe is illuminated by the field of the source, we need to express the cylindrical waves in Eq. (5) in terms of cylindrical waves defined in the probe coordinate system. To distinguish between the global coordinate system (in which the scan cylinder is given by $\rho=a$) and the probe coordinate system (in which the probe is fixed) we attach primes to all coordinates defined with respect to the probe coordinate system.

Assume that the reference point of the probe is at (a,ϕ_s,z_s) on the scan cylinder. Then we need to transform the cylindrical wave functions in Eq. (5) into cylindrical wave functions in the probe coordinate system, which is centered at (a,ϕ_s,z_s) with its x axis pointing toward the center of the global coordinate system. To achieve this transformation we use the rotation-translation formula for cylindrical wave functions

$$H_m^{(1)}(\rho)e^{im\phi}=(-1)^m e^{im\phi_s}\sum_{n=-\infty}^{+\infty}H_{n-m}^{(1)}(\rho_s)J_n(\rho')e^{in\phi'},\quad \rho_s>\rho', \tag{25}$$

where the primed quantities are defined in the probe coordinate system and the unprimed quantities are defined in the global coordinate system, as shown in Fig. 5.

Equation (25) can be inserted into expression (5) to get the following formula for the pressure on the scan cylinder:

$$p(a,\phi_s,z_s)=\sum_{m=-\infty}^{+\infty}(-1)^m e^{im\phi_s}\times\sum_{n=-\infty}^{+\infty}\int_{-\infty}^{+\infty}[J_n(k_\rho\rho')e^{in\phi'}e^{ik_z z'}]F_m(k_z)H_{n-m}^{(1)}\times(k_\rho a)e^{ik_z z_s}dk_z, \tag{26}$$

which expresses the outgoing waves that emanate from the source in the global coordinate system in terms of standing waves $J_n(k_\rho\rho')e^{in\phi'}e^{ink_z z'}$ in the probe coordinate system. From the definition of the probe receiving coefficients, we see that the total probe output is

$$b_p(a,\phi,z)=\sum_{m=-\infty}^{+\infty}(-1)^m e^{im\phi_s}\sum_{n=-\infty}^{+\infty}\int_{-\infty}^{+\infty}C_n(k_z)F_m(k_z)H_{n-m}^{(1)}\times(k_\rho a)e^{ik_z z_s}dk_z. \tag{27}$$

The expression (27) is easily inverted by use of the orthogonality relations (9) and (10) to get the final probe-corrected expression for the spectrum

$$F_m(k_z)=D_m(k_z)I_m(k_z), \tag{28}$$

where

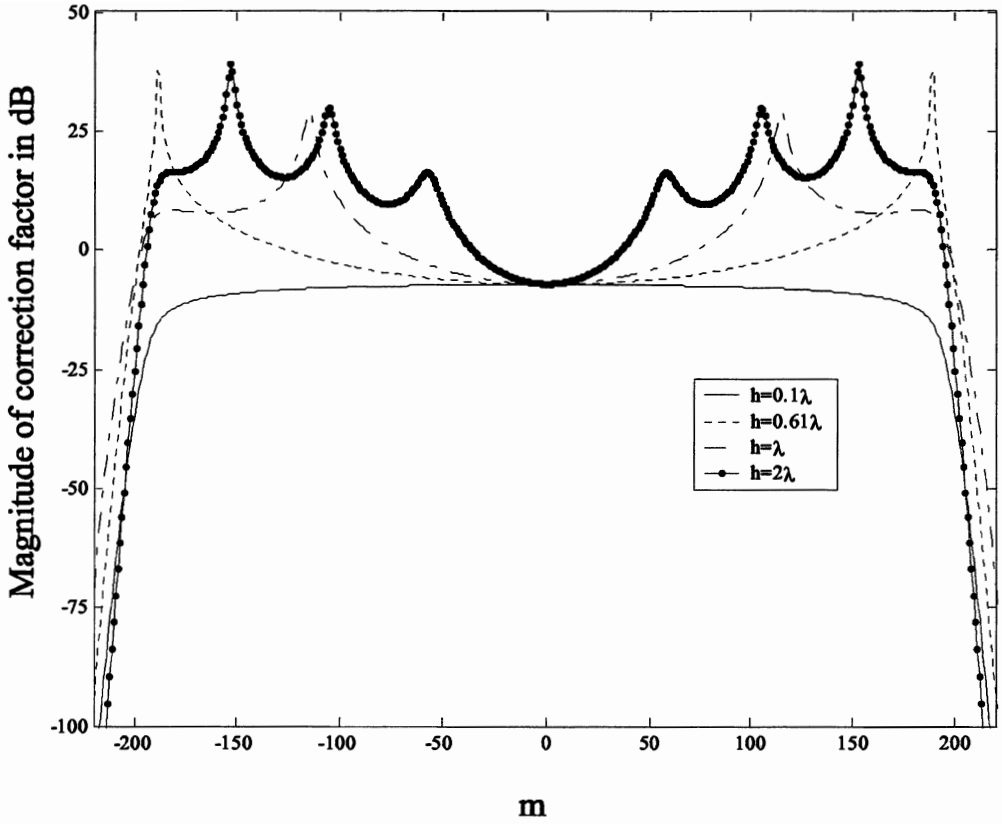

FIG. 6. Correction factor at $k_z=0$ for piston probes with $h=0.1\lambda$, $h=0.61\lambda$, $h=\lambda$, and $h=2\lambda$ that measure the field on a scan cylinder of radius $a-30\lambda$.

$$I_m(k_z)=\int_{-\infty}^{+\infty}\int_0^{2\pi} b_p(a,\phi_s,z_s)e^{-im\phi_s}e^{-ik_z z_s}d\phi_s dz_s \tag{29}$$

is a Fourier integral of the probe output over the scan cylinder and

$$D_m(k_z)=\frac{(-1)^m}{4\pi^2\sum_{n=-\infty}^{+\infty} C_n(k_z)H^{(1)}_{n-m}(k_\rho a)} \tag{30}$$

is a correction factor that depends on the probe receiving coefficients and the scan cylinder radius. The far field of the source is expressed in Eq. (6) in terms of the expansion coefficients $F_m(k_z)$ evaluated at $k_z=k\cos\theta$, and the formula (16) determines the probe receiving coefficients $C_n(k_z)$ in terms of the plane-wave receiving characteristic of the probe. For an ideal probe whose output equals the pressure ($C_n=0$ for $n\neq 0$ and $C_0=1$), Eq. (28) reduces correctly to the nonprobe-corrected formula (8).

Figure 6 shows the magnitude in decebels of the correction factor (30) for piston probes with $h=0.1\lambda$, $h=0.61\lambda$, $h=\lambda$, and $h=2\lambda$. The scan cylinder radius is $a=30\lambda$ and the observation direction is $\theta=90°$, corresponding to $k_z=0$. We shall now describe how the correction factor corrects for the probe pattern for far-field observation points near $\theta=\pi/2$.

First assume that the field is produced by a point source at the origin so that $R_{\min}=0$. Then the expansion coefficients $F_m(0)$ are zero for $m\neq 0$, and only the correction factor $D_0(0)$ comes into play. For points on the scan cylinder near the x-y plane, the output is roughly the same for all four probes because the point source is in the direction of the main beam (see Fig. 3 with $\beta=0$). The far field of the point source at $\theta=\pi/2$ is mainly determined by the probe output near the x-y plane, so the correction factor $D_0(0)$ should be roughly the same for the four probes, as confirmed by Fig. 6.

Next assume that the field is produced by a point source on the x axis at $x=3a/4$, for which the expansion coefficients $F_m(0)$ with $|m|<150$ are non-negligible. The probe sees this point source at an angle $\beta=37°$ when the probe is at $(x,y,z)=(0,a,0)$ and $(x,y,z)=(0,-a,0)$. At all other observation points in the x-y plane, the probes sees the point scatterer at an angle β that is less than 37°. Consider the piston probe with $h=\lambda$. From Fig. (3) we see that $\beta=37°$ is near the first null of this probe, so very low outputs are obtained when the probe is near $(x,y,z)=(0,a,0)$ and $(x,y,z)=(0,-a,0)$. To compensate for these low outputs, the correction factor $D_m(0)$ has a peak at $|m|=120$ and attains large values around this peak. Hence, to compute some of the higher-order expansion coefficients of the source $F_m(0)$, the integral over the scan cylinder $I_m(0)$ must be boosted by a large correction factor $D_m(0)$. These arguments can be repeated for the other piston probes in Fig. 3.

This discussion shows that nulls and low sidelobe levels in the probe receiving pattern result in large values of the correction factor. Correction factors that vary significantly with m, can often lead to errors in the computed far field because some of the higher-order expansion coefficients of the source F_m are computed as the product of a small number that can be relatively inaccurate (the integral of the probe output over the scan cylinder I_m) and a very large number

(the correction factor D_m). Therefore, it is advantageous to avoid probes that have nulls and low sidelobe levels in the region of the sources.

In Sec. IV we show how the far field can be computed from sampled values of the probe output on the scan cylinder. If the angular sampling rate is $\Delta\phi$, the far-field summation (6) includes the terms with $|n| < \pi/\Delta\phi$ (recall that the spectrum in Eq. (6) is given in Eq. (28) as $F_n = D_n I_n$). Hence, by decreasing the sample spacing $\Delta\phi$ the far-field error may increase because more of the peaks of the correction factor are included. This phenomenon is illustrated in Sec. V. Of course, the sample rate $\Delta\phi$ must always be chosen small enough to properly resolve the field of the source.

We shall now briefly discuss an approximate probe-corrected formula obtained by inserting[35]

$$H^{(1)}_{n-m}(k_\rho a) \simeq (-1)^m (-i)^n e^{-in \arcsin(m/[k_\rho a])} H^{(1)}_m(k_\rho a) \quad (31)$$

into Eq. (30) to get

$$D_m(k_z) \simeq \frac{1}{4\pi^2 R_p(k_p \cos[\arcsin(m/[k_\rho a]) + \pi], k_\rho \sin[\arcsin(m/[k_\rho a]) + \pi]) H^{(1)}_m(k_\rho a)}. \quad (32)$$

An electromagnetic analog of Eq. (32) was derived by Borgiotti[9,10] and subsequently rederived by Yaghjian.[8] The approximate formula (32) expresses the correction factor $D_m(k_z)$ directly in terms of the receiving characteristic $R_p(k_x, k_y)$ and avoids the use of the cylindrical receiving coefficients $C_n(k_z)$ that occur in the exact formula (30). By invoking the relation (13), the formula (32) expresses the correction factor directly in terms of the probe far-field pattern. For $k_\rho a \gg 1$, expression (31) is accurate only for small $|n|$ and values of $|m|$ that are not too close to $k_\rho a$. Hence, Eq. (32) is accurate only for small probes with only a few nonzero receiving coefficients $C_n(k_z)$ and for sources with $R_{\min}$ not too close to a. The approximate formula (32) is singular when $\arcsin(m/[k_\rho a]) + \pi$ coincides with a null of the receiving characteristic. These singularities correspond to the "peaks" discussed above where the exact correction factor attains large values but remains finite. The approximate formula (32) thus fails to correctly predict the values of the correction factor near its peaks. However, it is a valuable formula that avoids the use of the cylindrical receiving coefficients and produces accurate far fields for small probes whose patterns are null free. As we shall demonstrate below, small probes have additional advantages.

The fact that the exact correction factor is without singularities distinguishes cylindrical scanning from planar scanning: In planar scanning the exact correction factor is proportional to $1/R_p$ and thus has singularities at the nulls of R_p, as proven by Hansen and Yaghjian[5]. This discussion was confined to far-field observation directions near $\theta = \pi/2$. In Sec. V we shall show how nulls in the probe pattern affects the computed far field for observation points away from $\theta = \pi/2$.

III. TRUNCATION OF THE SCAN CYLINDER

The exact expressions (8) and (28)–(30) for the expansion coefficients $F_m(k_z)$ involve an integration over an entire infinite scan cylinder of either the pressure or the probe output. Practical near-field measurements are carried out only over a truncated scan cylinder, which we assume is given by $-z_0 \leq z \leq z_0$ and $\phi_0 \leq \phi \leq 2\pi - \phi_0$, where $z_0 > 0$ and $0 \leq \phi_0 < \pi$. The near-field data required by Eqs. (8) and (28)–(30) is therefore not available in practice. Fortunately, experience has shown that very accurate far fields can be obtained in certain regions from measurements on a truncated scan cylinder. In this section we shall study the errors caused by truncation and develop methods for reducing them. Truncation in the z and ϕ directions are considered in Secs. III A and III B, respectively.

First we state a result from Hansen *et al.*[22] that restricts the range of observation angles for which we can accurately compute the far field from a truncated scan: *If the scanned area is thought of as a transparent surface and the rest of the infinite scan cylinder is opaque, then accurate far fields can be achieved only in directions from which one can see the entire source region.* Similar results have been cited for planar and spherical scanning surfaces.[36–39]

A. Truncation in the z direction

Typically the field outside the scanned area is neglected and the exact expression (29) is approximated by

$$I_n(k_z) \simeq \int_{-z_0}^{z_0} \int_{\phi_0}^{2\pi-\phi_0} b_p(a, \phi_s, z_s) e^{-in\phi_s} e^{-ik_z z_s} d\phi_s dz_s. \quad (33)$$

It is thus assumed that the contribution to the integral (29) from the region not covered by the scan is negligible. For cylindrical near-field measurements of directive transducers this assumption is often valid because the measurements are set up so that very little energy is radiated in directions not covered by the truncated scan cylinder. However, a nondirective transducer or a scatterer may radiate significantly in all directions, including the ones that are not covered by the scan cylinder. Hence, it is not always a valid approximation to neglect the contribution to the integral in Eq. (29) from the region not covered by the scan.

We shall next present two sets of asymptotic correction formulas that approximate the contribution from the region of the scan cylinder with $|z| > z_0$. Detailed derivations can be

found in Hansen *et al.*[22] First we assume that the field on the scan cylinder behaves roughly as a plane wave $e^{ik|z|}$ as $z \to \pm\infty$ and find that

$$I_n(k_z) \simeq \int_{-z_0}^{z_0}\int_{\phi_0}^{2\pi-\phi_0} b_p(a,\phi_s,z_s)e^{-in\phi_s}e^{-ik_z z_s}d\phi_s dz_s - \frac{e^{ik_z z_0}}{i(k+k_z)}\int_{-\phi_0}^{2\pi-\phi_0} b_p(a,\phi_s,-z_0)e^{-in\phi_s}d\phi_s - \frac{e^{-ik_z z_0}}{i(k-k_z)}\int_{\phi_0}^{2\pi-\phi_0} b_p(a,\phi_s,z_0)e^{-in\phi_s}d\phi_s. \quad (34)$$

We use the term "edge-corrected" formula because the integral over the uncovered areas of the infinite scan cylinder are approximated by integrations along the top and bottom edges of the truncated scan cylinder.

The second set of correction formulas assumes that field behaves as a spherical wave e^{ikr} as $z \to \pm\infty$. The edge-corrected formula for the spherical-wave assumption is[40]

$$I_n(k_z) \simeq \int_{-z_0}^{z_0}\int_{\phi_0}^{2\pi-\phi_0} b_p(a,\phi_s,z_s)e^{-in\phi_s}e^{-ik_z z_s}d\phi_s dz_s - \frac{e^{ik_z z_0}}{i(k\cos\theta_0+k_z)}\int_{\phi_0}^{2\pi-\phi_0} b_p(a,\phi_s,-z_0)e^{-in\phi_s}d\phi_s - \frac{e^{-ik_z z_0}}{i(k\cos\theta_0-k_z)}\int_{\phi_0}^{2\pi-\phi_0} b_p(a,\phi_s,z_0)e^{-in\phi_s}d\phi_s, \quad (35)$$

where $\cos\theta_0 = z_0/\sqrt{a^2+z_0^2}$. Note that the edge-corrected formula (35) is singular for far-field observation directions with $\theta=\theta_0$ and $\theta=\pi/2-\theta_0$. This follows from the far-field expression (6) which shows that the far field in the direction (θ,ϕ) is determined from the spectrum evaluated at $k_z=k\cos\theta$. The edge-corrected formula (34) does not have these singularities.

B. Truncation in the ϕ direction

For the angular truncation of the scan cylinder we cannot derive asymptotic correction formulas similar to Eqs. (34) and (35) because no asymptotic expression suggests itself for the ϕ dependence of the field. Indeed, the ϕ dependence of the field on the scan cylinder depends strongly on the source shape, so we do not have a general expression for $b_p(a,\phi,z)$ that holds when ϕ is outside the scanned region $\phi_0 \leq \phi \leq 2\pi-\phi_0$.

To determine the effect of ϕ truncation, insert the formula (28) for the spectrum $F_m(k_z)$ into the far-field formula (6) to get

$$p(r,\theta,\phi) \sim \frac{e^{ikr}}{r}\int_{-\infty}^{+\infty}\int_0^{2\pi} b_p(a,\phi_s,z_s)G(k,a,\theta,\phi - \phi_s;\{C_n\})e^{-ikz_s\cos\theta}d\phi_s dz_s, \quad (36)$$

where

$$G(k,a,\theta,\phi;\{C_n\}) = \sum_{m=-\infty}^{+\infty}\frac{(-1)^m e^{-i(m+1)\pi/2}e^{im\phi}}{2\pi^2\sum_{n=-\infty}^{+\infty} C_n(k\cos\theta)H_{n-m}^{(1)}(ka\sin\theta)} \quad (37)$$

will be called the taper function. Equation (36) expresses the far field of the source directly in terms of an integration over the scan cylinder of the probe output multiplied by the taper function. This expression is useful for determining the ϕ-truncation errors but not efficient for actually computing the far field since the fast Fourier transform (FFT) cannot be fully exploited. We shall now examine the taper function (37) for an ideal probe and for piston probes.

1. Ideal probe

For an ideal probe ($C_n=0$ for $n\neq 0$ and $C_0=1$), the taper function (37) reduces to

$$G_i(ka,\theta,\phi) = \sum_{m=-\infty}^{+\infty}\frac{e^{-i(m+1)\pi/2}e^{im\phi}}{2\pi^2 H_m^{(1)}(ka\sin\theta)}. \quad (38)$$

The piston probe with $h=0.1\lambda$ is approximately an ideal probe. By inspection, we see that the function $G_i(ka,\theta,\phi-\phi_s)e^{-ikz_s\cos\theta}$ equals the total field on a hard circular cylinder that is illuminated by a plane wave with amplitude $(2\pi i)^{-1}ka\sin\theta$ that propagates in the $-\hat{\mathbf{r}}$ direction. Here, $\hat{\mathbf{r}}$ is the unit vector for the far-field observation direction. Hence, *the far field of the source is obtained by integrating over the scan cylinder the product of the near field of the source and the total field on a hard cylinder, which coincides with the scan cylinder and is illuminated by a plane wave that originates at the far-field observation point.*

Jones[41] used the Watson transform to prove that as $ka\sin\theta \to \infty$ the function $G_i(ka,\theta,\phi)$ decays exponentially for $\pi/2 < |\phi| \leq \pi$, has a transition zone around $|\phi|=\pi/2$, and behaves as

$$G_i(ka,\theta,\phi) \sim \left[\frac{ka\sin\theta}{2\pi i}\right]\cos\phi e^{-ika\sin\theta\cos\phi}, \quad |\phi| < \pi/2, \quad ka\sin\theta \to +\infty. \quad (39)$$

Figure 7 shows $G_i(ka,\theta,\phi)$ and its asymptotic approximation (39) for $ka\sin\theta=25$. The asymptotic approximation works well even at this low value of $ka\sin\theta$.

The qualitative behavior of $G_i(ka,\theta,\phi)$ plotted in Fig. 7 for $ka\sin\theta=25$ remains the same for all larger $ka\sin\theta$. Hence, the far-field formula (36) shows that the field in a given direction with angle ϕ is determined by integrating the field on the scan cylinder multiplied by an oscillating function of ϕ_s that is symmetric and decays away from $\phi_s=\phi$. In other words, the cylindrical wave-function expansion of the far field automatically applies an angular taper function to the field on the scan cylinder. No taper function is applied for the z_s dependence. The asymptotic expression (39) shows that the oscillations increase in frequency with increasing $ka\sin\theta$.

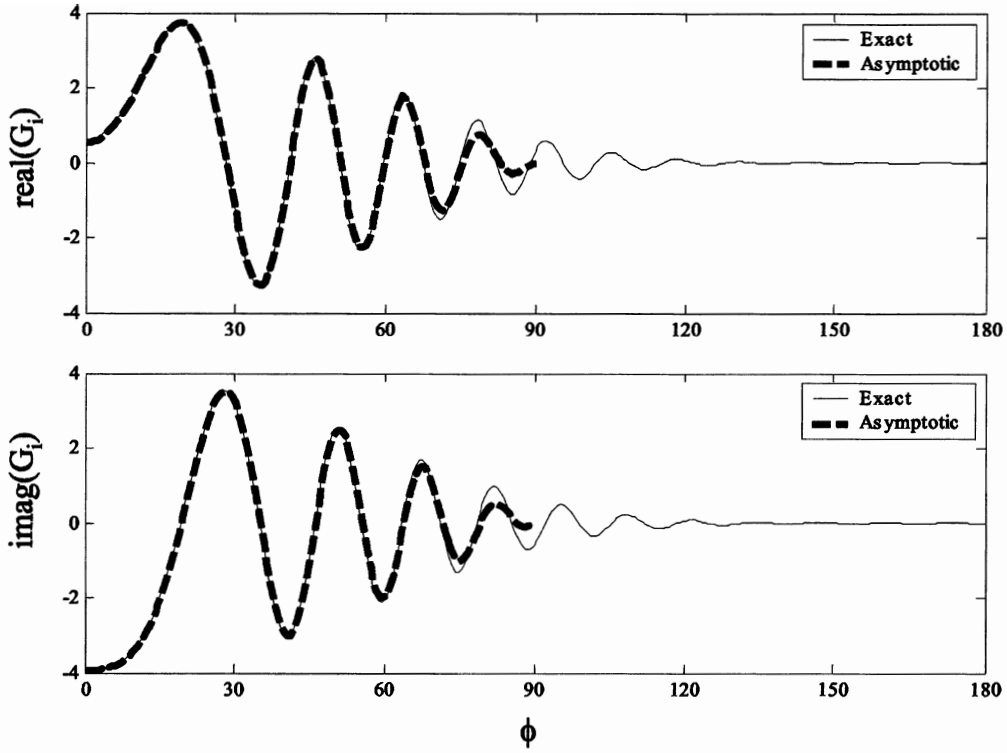

FIG. 7. Real (top) and imaginary (bottom) parts of the function G_i and its asymptotic approximation for $ka \sin\theta=25$.

2. Piston probe

Figure 8 shows an upper envelope of the taper function in Eq. (37) for piston probes with $h=0.1\lambda$, $h=0.61\lambda$, $h=\lambda$, and $h=2\lambda$. The scan cylinder radius is $a=30\lambda$ and the observation direction is $\theta=90°$, corresponding to $k_z=0$. To visualize the rapidly oscillating taper function, we computed an upper envelope that equals the maximum magnitude of the taper function over 5° intervals.

Let us first discuss the behavior of the taper function for $h=0.1\lambda$ (this piston probe is almost an ideal probe whose

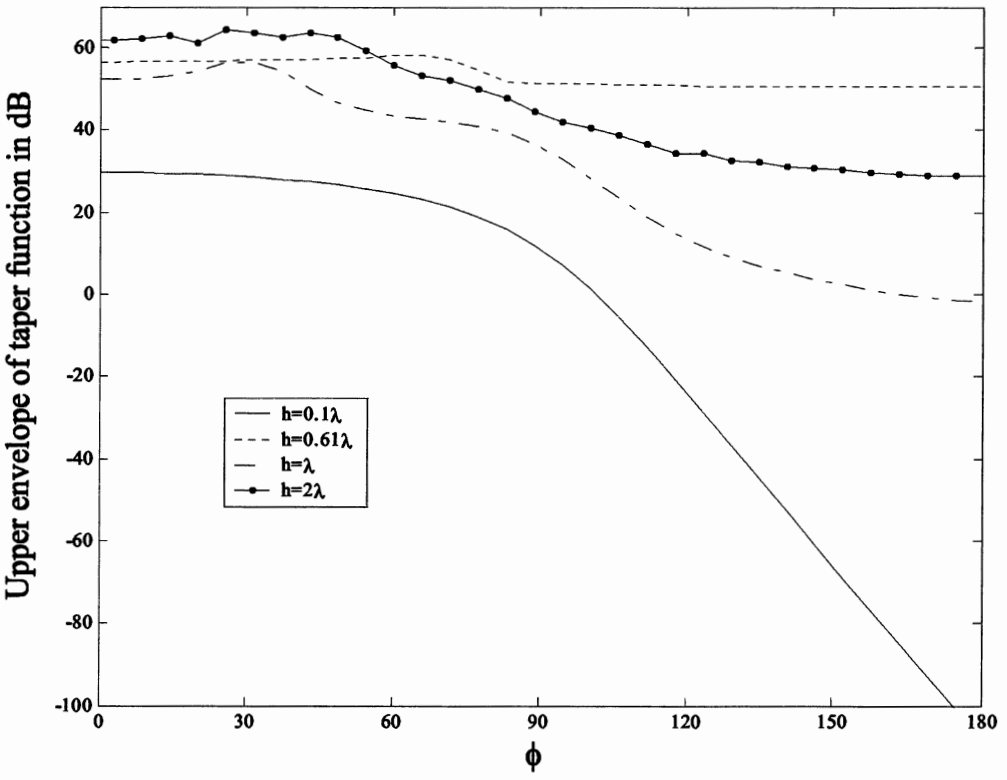

FIG. 8. Upper envelope of the taper functions for $a=30\lambda$ and $\theta=90°$ for piston probes with $h=0.1\lambda$, $h=0.61\lambda$, $h=\lambda$, and $h=2\lambda$. All non-negligible terms of the expansion for the taper function are included.

output equals the pressure). In the region from $\phi=0°$ to $\phi=90°$ the taper function decays at a moderate rate from 30 to about 5 dB. Beyond $\phi=90°$ the decay is exponential (creeping-wave region), and at $\phi=180°$ the magnitude of the taper function is below −100 dB. Hence, the probe output on the scan cylinder at points that lie more than 90° away from the far-field observation direction are attenuated by more than 25 dB when the fields are measured with a piston probe of radius $h=0.1\lambda$. We shall later see that the strong taper helps reduce truncation effects.

The taper functions for the piston probes with $h=0.61\lambda$, $h=\lambda$, and $h=2\lambda$ do not exhibit such rapid decay. For example, the taper function for the piston probe of radius $h=0.61\lambda$ decays only 5 dB over the entire range from $\phi=0°$ to $\phi=180°$, and thus only a mild taper is applied to the probe output. The values of the taper functions in Fig. 8 were computed from the summation (37) with all non-negligible terms included. For practical far-field calculations, the summation in Eq. (37) is truncated at a mode number determined by the size of the source region. This truncation of the summation strongly affects the taper function, as will be demonstrated in Sec. V.

C. Green's function representation

Let us briefly discuss a far-field formula that is based on the free-space Green's function rather than the cylindrical wave functions. From Hansen *et al.*[5] it follows that the far field can be expressed in terms of the pressure and its normal derivative on the scan cylinder as

$$p(r,\theta,\phi)\sim-\frac{iae^{ikr}}{4\pi r}\int_{-\infty}^{+\infty}\int_{0}^{2\pi}\left[ik\hat{\mathbf{r}}\cdot\hat{\boldsymbol{\rho}}'p(\mathbf{r}')+\frac{\partial}{\partial\rho'}p(\mathbf{r}')\right]e^{-ik\hat{\mathbf{r}}\cdot\mathbf{r}'}d\phi'dz'. \tag{40}$$

The normal derivative of the pressure can be related to the velocity by the formula $\partial/\partial\rho'\,p(\mathbf{r}')=i\omega\rho_{m0}\boldsymbol{\rho}'\cdot\mathbf{v}(\mathbf{r}')$, where ρ_{m0} is the mass density of the undisturbed fluid.

This formula is seldom used in near-field scanning because it requires that both the pressure and its normal derivative be measured. Unlike the formulas that are based on the cylindrical wave functions, the formula (40) does not apply an angular taper function to the field on the scan cylinder. Hence, angular truncations of the scan cylinder would in general affect Eq. (40) more than they affect formulas based on cylindrical wave functions.

IV. SAMPLING THEOREMS AND COMPUTATION SCHEMES

The formulas derived so far for the far field of the source involve integrations of the probe output over the scan cylinder and infinite summations over angular modes. In this section we discretize these formulas so that the far field of the source can be computed from a finite number of probe-output values sampled at regular intervals on the scan cylinder. As part of the discretization, we present sampling theorems that determine the sample spacing required for accurate far-field calculation.

The scan cylinder is truncated and given in cylindrical coordinates by $\rho=a$ and $|z|\leq z_0$, and the field on the scan cylinder is measured at the grid points expressed in terms of the cylindrical coordinates as

$$\phi=(\ell-1)\Delta\phi,\quad \ell=1,2,\ldots,N_\phi, \tag{41}$$

and

$$z=(m-1)\Delta z-z_0,\quad m=1,2,\ldots,N_z. \tag{42}$$

The formulas of this section require the probe over the entire 360° range. If the scan cylinder is angularly truncated, one simply inserts zeros into the array positions that correspond to measurement points that are outside the scanned area. Note that z_0 satisfies the relation $z_0=(N_z-1)\Delta z/2$.

If every point on the scan cylinder is at least one wavelength or so away from the nearest point on a nonresonant source,[42] the sampling intervals $\Delta\phi$ and Δz can be chosen as follows:[17]

$$\Delta\phi=\frac{2\pi}{N_\phi},\quad N_\phi=2\,\mathrm{int}(kR_{\min}+n_1), \tag{43}$$

$$\Delta z=\frac{\lambda}{2}, \tag{44}$$

where $R_{\min}$ is the radius of the minimum cylinder, n_1 is a small integer, and λ is the wavelength. In Eq. (43) the function "int" denotes the integer value.

The sampling theorems show that the infinite summation (6) can be replaced by the finite summation

$$p(r,\theta,\phi)\sim\frac{2e^{ikr}}{r}\sum_{n=-N_0}^{N_0}D_n(k\cos\theta)I_n(k\cos\theta)e^{in\phi}e^{-i\pi(n+1)/2}, \tag{45}$$

where $D_n(k\cos\theta)$ is the correction factor defined in Eq. (30), and N_0 is an integer that must be large enough to include all the significient modes of a give source region. When strong edge effects are present, N_0 should be large enough to prevent aliasing caused by the discontinuity of the near-field data at the truncation edges.[22] Since only the values of $I_n(k\cos\theta)$ with $|n|\leq N_\phi/2$ can be computed accurately, one must chose $N_0\leq N_\phi/2$.

Next we introduce the two-dimensional array

$$\tilde{b}_p(\ell,m)=b_p(a,(\ell-1)\Delta\phi,(m-1)\Delta z-z_0),$$

$$\ell=1,2,\ldots,N_\phi,\quad m=1,2,\ldots,N_z, \tag{46}$$

which contains the probe output b_p at the grid points. A straightforward discretization of the formula (33) for the spectrum then gives

$$I_n(k_z)=\Delta z\Delta\phi e^{ik_zz_0}\sum_{\ell=1}^{N_\phi}\sum_{m=1}^{N_z}e^{-in\Delta\phi(\ell-1)}e^{-ik_z\Delta z(m-1)}\tilde{b}_p(\ell,m). \tag{47}$$

Note that both the far-field formula (45) and the probe-corrected formula (47) for the spectrum can be computed efficiently with the FFT.

We can also discretize the edge-corrected formulas (34) and (35) to get

$$I_n(k_z) = \Delta z \Delta\phi e^{ik_z z_0} \sum_{\ell=1}^{N_\phi} \sum_{m=1}^{N_z} e^{-in\Delta\phi(\ell-1)} e^{-ik_z \Delta z(m-1)} \tilde{b}_p(\ell,m)$$
$$- \frac{\Delta z \Delta\phi e^{ik_z z_0}}{2} \sum_{\ell=1}^{N_\phi} e^{-in\Delta\phi(\ell-1)} \tilde{b}_p(\ell,1)$$
$$- \frac{\Delta z \Delta\phi e^{-ik_z z_0}}{2} \sum_{\ell=1}^{N_\phi} e^{-in\Delta\phi(\ell-1)} \tilde{b}_p(\ell,N_z)$$
$$- \frac{\Delta\phi e^{ik_z z_0}}{i(k+k_z)} \sum_{\ell=1}^{N_\phi} e^{-in\Delta\phi(\ell-1)} \tilde{b}_p(\ell,1)$$
$$- \frac{\Delta\phi e^{-ik_z z_0}}{i(k-k_z)} \sum_{\ell=1}^{N_\phi} e^{-in\Delta\phi(\ell-1)} \tilde{b}_p(\ell,N_z) \quad (48)$$

when the field is assumed to behave as $e^{ik|z|}$, and

$$I_n(k_z) = \Delta z \Delta\phi e^{ik_z z_0} \sum_{\ell=1}^{N_\phi} \sum_{m=1}^{N_z} e^{-in\Delta\phi(\ell-1)} e^{-ik_z \Delta z(m-1)} \tilde{b}_p(\ell,m)$$
$$- \frac{\Delta z \Delta\phi e^{ik_z z_0}}{2} \sum_{\ell=1}^{N_\phi} e^{-in\Delta\phi(\ell-1)} \tilde{b}_p(\ell,1)$$
$$- \frac{\Delta z \Delta\phi e^{-ik_z z_0}}{2} \sum_{\ell=1}^{N_\phi} e^{-in\Delta\phi(\ell-1)} \tilde{b}_p(\ell,N_z)$$
$$- \frac{\Delta\phi e^{ik_z z_0}}{i(k\cos\theta_0 + k_z)} \sum_{\ell=1}^{N_\phi} e^{-in\Delta\phi(\ell-1)} \tilde{b}_p(\ell,1)$$
$$- \frac{\Delta\phi e^{-ik_z z_0}}{i(k\cos\theta_0 - k_z)} \sum_{\ell=1}^{N_\phi} e^{-in\Delta\phi(\ell-1)} \tilde{b}_p(\ell,N_z) \quad (49)$$

when the field is assumed to behave as e^{ikr} and $\cos\theta_0 = z_0/\sqrt{a^2+z_0^2}$. The second and third in Eqs. (48) and (49) ensure that the contributions from the top and bottom edges are included only once. The number of operations required to compute the spectrum from any one of the formulas (47)–(49) is on the order of $N_\phi N_z \log_2(N_\phi, N_z)$. Hence, the edge-correction terms do not significantly add to the computational effort.

V. FAR-FIELD ERRORS FOR A POINT SOURCE

In this section we shall compute the far field of an acoustic point source from near-field measurements on a truncated scan cylinder. The field is measured with piston probes of varying size and the probe output is computed from the exact formula (22). Hence, if the scan cylinder is untruncated, the computed far field equals the exact far field, regardless of the size of the piston probe. The acoustic field is generated by a single point source (i.e., a nondirective source) located inside the scan cylinder, so the truncation edges of the scan cylinder are illuminated by relatively strong fields, and the truncation effects will be clearly visible. The scan cylinder is given by $a=30\lambda$ and $-40\lambda < z < 39.5\lambda$. Throughout, the sampling spacing in z is $\Delta z = \lambda/2$. First assume that the point source is located at $\mathbf{r}_s = 12\lambda\hat{\mathbf{y}} - 5\lambda\hat{\mathbf{z}}$.

TABLE I.

Average far-field error over the region $0 \leq \phi < 2\pi$ for $\theta = \pi/2$	$h=0.1\lambda$ (%)	$h=0.61\lambda$ (%)	$h=\lambda$ (%)	$h=2\lambda$ (%)
No edge correction	3.1	0.7	0.5	0.3
Plane-wage edge correction	0.9	0.2	0.1	0.1
Spherical-wave edge correction	1.3	0.2	0.2	0.1

We begin by investigating the improvements in far-field accuracy achieved with the formulas that correct for the truncations at the top and bottom edges of the scan cylinder. We let the scan cylinder be untruncated in ϕ and chose $N_\phi = 360$ corresponding to an angular sample spacing of $\Delta\phi = 1°$. (With $R_{\min} = 12\lambda$, the required sample spacing is about 2.3°.) The sample spacing in z is $\Delta z = \lambda/2$. We shall compare the far fields obtained with four different probe sizes: $h = 0.1\lambda$, $h = 0.61\lambda$, $h = \lambda$, and $h = 2\lambda$. The exact far field of a single point source located at $\mathbf{r}_s$ is

$$p_0(\mathbf{r}) \sim e^{-ik\hat{\mathbf{r}}\cdot\mathbf{r}_s} \frac{e^{ikr}}{r}. \quad (50)$$

Table I shows the average error of the far field for $\theta = \pi/2$ and $0 \leq \phi < 2\pi$ computed from this z-truncated scan using Eqs. (47)–(49).

We see that the edge-correction formulas significantly reduce the far-field error for all sizes of the piston probe. Moreover, the error is smaller for directive probes because of the reduced magnitude of the probe output near the top and bottom edges of the scan cylinder. In the remainder of this section we employ the edge-corrected formula (48) based on the plane-wave assumption.

Figure 9 shows the far-field error as a function of θ for $\phi = 0$ with the scan cylinder still untruncated in ϕ. The error is calculated at the angles $\theta = \arccos(k_z/k)$ with increments of k_z/k equal to 0.0125 (these increments automatically come out of the FFT when the sample spacing in z is $\lambda/2$ and no zero padding is applied). The vertical solid lines in Fig. 9 are the limiting angles at which the line that begins at the point source and ends at the far-field observation point touches the upper and lower truncation edges of the scan cylinder. As expected, outside these limiting angles the far-field error is so large that the computed far field is useless.

The far-field error curves have spikes that correspond to nulls in the probe patterns (see Fig. 3). These spikes are not exactly symmetric because the point source is not in the x-y plane. They result from the fact that the probe output is very small at values of z for which the point source is near the direction of a null. When the far field is computed in the corresponding θ direction, the correction factor is large and thus the errors caused by z truncation lead to an inaccurate value for the far field.

We now compute the far field of the point source at $\theta = \pi/2$ from measurements over the ϕ–z truncated scanning

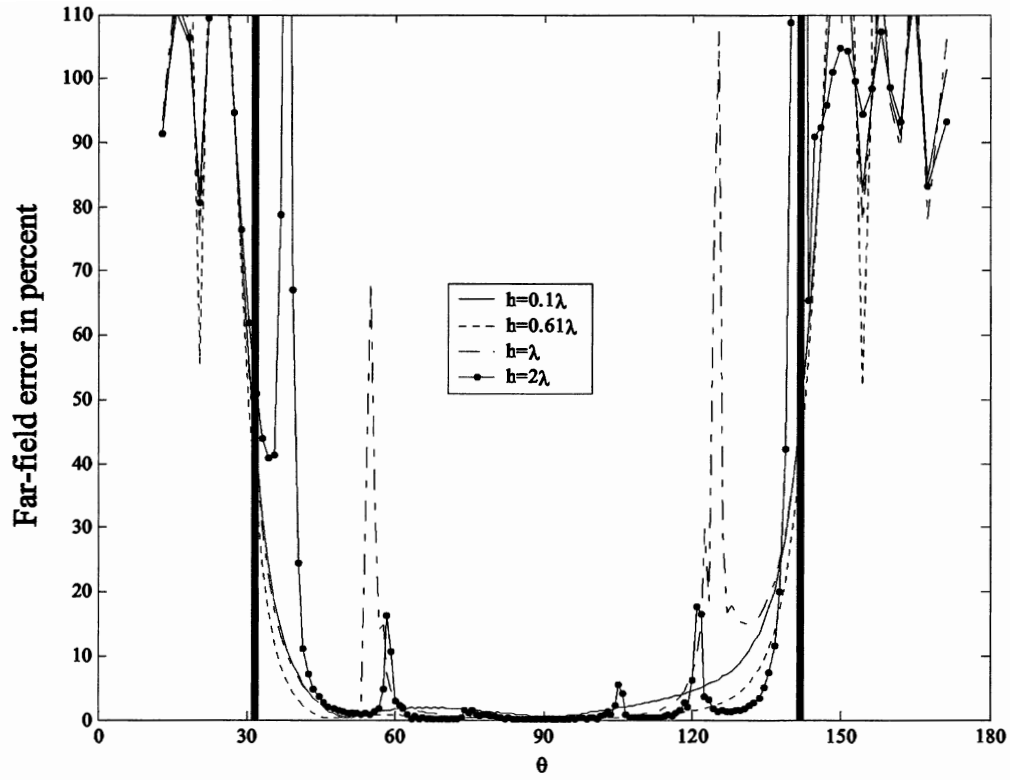

FIG. 9. Far-field error at $\phi=0°$ computed from a z-truncated scan with $a=30\lambda$, $0<\phi<360°$, and $-40\lambda<z<39.5\lambda$. The far-field error is calculated at $\theta=\arccos(k_z/k)$ with increments of k_z/k equal to 0.0125. The limiting angles in θ are indicated with vertical solid lines. The field is produced by a single point source at $(x,y,z)=(0,12\lambda,-5\lambda)$.

area given by $a=30\lambda$, $-40\lambda<z<39.5\lambda$, and $60°<\phi<300°$. Figure 10 shows this scanning area as a solid circular arc. We shall compute the far field with two different angular sampling spacings: (i) $\Delta\phi=1°$ resulting in $N_\phi=360$, and (ii) $\Delta\phi=2°$ resulting in $N_\phi=180$. Hence, the relevant taper functions are given by the summation in Eq. (37) truncated at $|m|=180$ and $|m|=90$. Figure 11 shows upper envelopes of these taper functions for piston probes with h

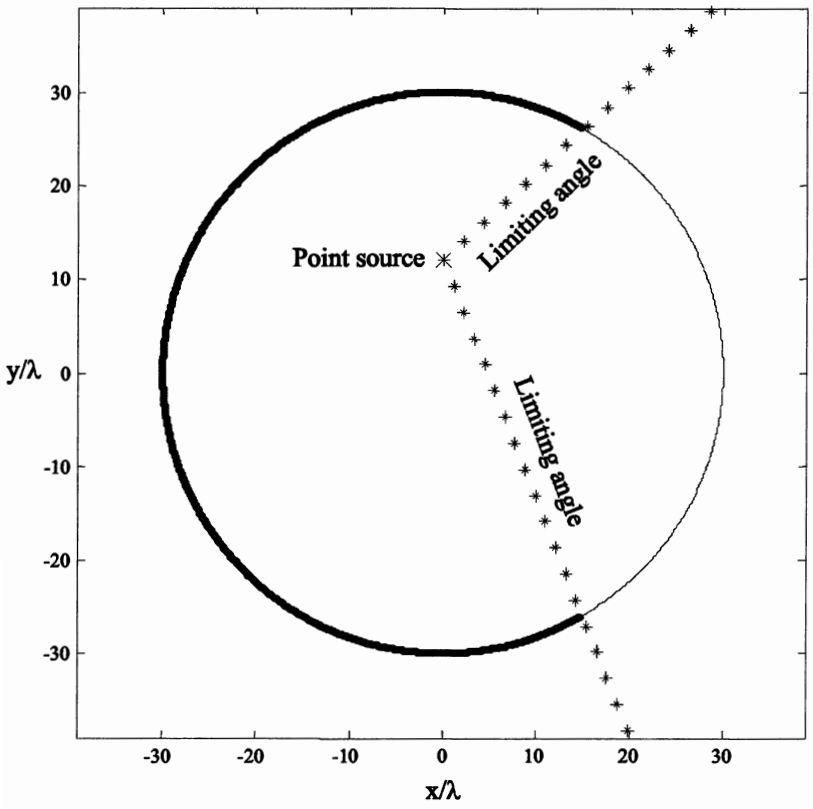

FIG. 10. Truncated scan cylinder with radius $a=30\lambda$. The scanned region is the solid circular arc given by $60°<\phi<300°$. The point source is located at $(x,y,z)=(0,12\lambda,-5\lambda)$, and the two limiting angles are marked by *.

an arbitrary but known measuring antenna," Electron. Lett. **6**, 346–347 (1970).
[3]D. M. Kerns, "Scattering-matrix description and near-field measurements of electro-acoustic transducers," J. Acoust. Soc. Am. **57**, 497–507 (1975).
[4]D. M. Kerns, *Plane-Wave Scattering-Matrix Theory of Antennas and Antenna-Antenna Interactions* NBS Monograph 162 (US Government Printing Office, Washington D.C., 1981).
[5]T. B. Hansen and A. D. Yaghjian, *Plane-Wave Theory of Time-Domain Fields* (IEEE, New York, 1999).
[6]W. M. Leach and D. T. Paris, "Probe compensated near-field measurements on a cylinder," IEEE Trans. Antennas Propag. **AP-21**, 435–445 (1973).
[7]D. T. Paris, W. M. Leach, Jr., and E. B. Joy, "Basic Theory of probe-compensated near-field measurements," IEEE Trans. Antennas Propag. **AP-26**, 373–379 (1978).
[8]A. D. Yaghjian, *Near-Field Antenna Measurements on a Cylindrical Surface: a Source Scattering-Matrix Formulation*, NBS Technical Note 696 (revised) (National Bureau of Standards, Boulder, CO, 1977).
[9]G. V. Borgiotti, "An integral equation formulation for probe corrected far-field reconstruction from measurements on a cylinder," *IEEE Antenna Propagat. Soc. International Symposium Digest*, Stanford University, June 1977.
[10]G. V. Borgiotti, "Integral equation formulation for probe corrected far-field reconstruction from measurements on a cylinder," IEEE Trans. Antennas Propag. **26**, 572–578 (1978).
[11]F. Jensen, "Electromagnetic near-field far-field correlations," Ph.D. dissertation, Technical University of Denmark, Lyngby, Denmark, 1970.
[12]F. Jensen, "On the probe compensation for near-field measurements on a sphere," AEU **29**, 305–308 (1975).
[13]P. F. Wacker, "Near-field antenna measurements using a spherical scan: Efficient data reduction with probe correction," *IEE Conf. Publ. 113* (Conf. Precision Electromagn. Measurements, London, 1974), pp. 286–288.
[14]F. H. Larsen, "Probe Correction of spherical near-field measurements," Electron. Lett. **13**, 393–395 (1977).
[15]A. D. Yaghjian and R. C. Wittmann, "The receiving antenna as a linear differential operator: application to spherical near-field measurements," IEEE Trans. Antennas Propag. **AP-33**, 1175–1185 (1985).
[16]A. D. Yaghjian, "Simplified approach to probe-corrected spherical near-field scanning," Electron. Lett. **20**, 195–196 (1984).
[17]J. Hald, F. Jensen, and F. H. Larsen, *Spherical Near-Field Antenna Measurements*, edited by J. E. Hansen (Peter Peregrinus, London, 1988).
[18]R. C. Wittmann, "Probe-corrected spherical near-field scanning in acoustics," IEEE Trans. Instrum. Meas. **41**, 17–21 (1992).
[19]T. B. Hansen, "Formulation of spherical near-field scanning for time-domain acoustic fields," J. Acoust. Soc. Am. **98**, 1204–1215 (1995).
[20]T. B. Hansen, "Formulation of spherical near-field scanning for time-domain electromagnetic fields," IEEE Trans. Antennas Propag. **45**, 620–630 (1997).
[21]M. G. Cote and R. M. Wing, "Demonstration of bistatic electromagnetic scattering measurements by spherical near-field scanning," *Proc. AMTA Symposium* (Dallas, TX, 1963), p. 191.
[22]T. B. Hansen, R. A. Marr, U. H. W. Lammers, T. J. Tanigawa, and R. V. McGahan (unpublished).
[23]R. A. Marr, U. H. W. Lammers, T. B. Hansen, T. J. Tanigawa, and R. V. McGahan (unpublished).
[24]B. P. Hildebrand and B. B. Brenden, *An Introduction to Acoustical Holography* (Plenum Press, New York, 1974).
[25]E. G. Williams and J. D. Maynard, "Holographic Imaging without the Wavelength Resolution limit," Phys. Rev. Lett. **45**, 554–557 (1980).
[26]E. G. Williams, H. D. Hardy, and R. G. Fink, "Nearfield Acoustical Holography using an Underwater, Automated Scanner," J. Acoust. Soc. Am. **78**, 789–798 (1985).
[27]E. G. Williams, *Fourier Acoustics: Sound Radiation and Nearfield Acoustical Holography* (Academic Press, New York, 1999).
[28]J. A. Stratton, *Electromagnetic Theory* (McGraw-Hill, New York, 1941), sec. 7.2.
[29]N. Bleistein and R. A. Handelsman, *Asymptotic Expansions of Integrals* (Dover, New York, 1986), p. 220.
[30]A. D. Yaghjian, "Generalized or adjoint reciprocity relations for electroacoustic transducers," J. Res. Natl. Bur. Stand., Sect. B **79B**, 17–39 (1975).
[31]H. Weyl, "Ausbreitung elektromagnetischer Wellen uber einem ebenen Leiter," Ann. Phys. **60**, 481–500 (1919).
[32]L. V. King, Can. J. Res. **11**, 135–146 (1934).
[33]G. R. Harris, "Review of transient field theory for a baffled planar piston," J. Acoust. Soc. Am. **70**, 10–20 (1981).
[34]E. B. Miller and A. D. Yaghjian, "Two theoretical results suggesting a method for calibrating ultrasonic transducers by measuring the total nearfield force," J. Acoust. Soc. Am. **66**, 1601–1608 (1979).
[35]H. Jeffreys, *Asymptotic Approximations* (Clarendon Press, Oxford, 1962), sec. 4.3.
[36]A. D. Yaghjian, *Upper-Bound Errors in Far-Field Antenna Parameters Determined from Planar Near-Field Measurements*, NBS Technical Note 667 (National Bureau of Standards, Boulder, CO, 1975).
[37]A. C. Newell, "Error analysis techniques for planar near-field measurements," IEEE Trans. Antennas Propag. **36**, 754–768 (1988).
[38]E. B. Joy and A. D. Dingsor, "Computer simulation of cylindrical surface near-field measurement system errors," *IEEE Antenna Propagat. Soc. International Symposium Digest*, Seattle, WA, 1979, pp. 565–568.
[39]F. Jensen, "Computer simulations as a design tool in near-field testing," *IEE Conf. Publ. 169, Pt. 1*, Seattle, WA, 1978, pp. 111–114.
[40]A. D. Yaghjian (private communication, 2002).
[41]D. S. Jones, *Acoustic and Electromagnetic Waves* (Clarendon Press, Oxford, 1986), pp. 417–421.
[42]A. D. Yaghjian, "Sampling criteria for resonant antennas and scatterers," J. Appl. Phys. **79**, 7474–7482 (1996); A. D. Yaghjian, Erratum **79**, 2547(E) (1996).